

## Numerical assessment of step-by-step integration methods in the paradigm of real-time hybrid testing

Mohit Verma<sup>\*1,2</sup>, J. Rajasankar<sup>1,2a</sup> and Nagesh R. Iyer<sup>1b</sup>

<sup>1</sup>Academy of Scientific and Innovative Research, New Delhi, India

<sup>2</sup>CSIR-Structural Engineering Research Centre, Chennai, India

(Received June 26, 2013, Revised January 16, 2015, Accepted February 16, 2015)

**Abstract.** Real-time hybrid testing (RTHT) involves virtual splitting of the structure into two parts: physical substructure that contains the key region of interest which is tested in a laboratory and numerical substructure that contains the remaining part of the structure in the form of a numerical model. This paper numerically assesses four step-by-step integration methods (Central difference method (CDM), Operator splitting method (OSM), Rosenbrock based method (RBM) and CR-integration method (CR)) which are widely used in RTHT. The methods have been assessed in terms of stability and accuracy for various realistic damping ratios of the physical substructure. The stability is assessed in terms of the spectral radii of the amplification matrix while the accuracy in terms of numerical damping and period distortion. In order to evaluate the performance of the methods, five carefully chosen examples have been studied - undamped SDOF, damped SDOF, instantaneous softening, instantaneous hardening and hysteretic system. The performance of the methods is measured in terms of a non-dimensional error index for displacement and velocity. Based on the error indices, it is observed that OSM and RBM are robust and performs fairly well in all the cases. CDM performed well for undamped SDOF system. CR method can be used for the system showing softening behaviour. The error indices indicate that accuracy of OSM is more than other method in case of hysteretic system. The accuracy of the results obtained through time integration methods for different damping ratios of the physical substructure is addressed in the present study. In the presence of a number of integration methods, it is preferable to have criteria for the selection of the time integration scheme. As such criteria are not available presently, this paper attempts to fill this gap by numerically assessing the four commonly used step-by-step methods.

**Keywords:** performance assessment; real-time hybrid testing; step-by-step integration; stability; accuracy

### 1. Introduction

Real-time hybrid testing (RTHT) is based on the concept of structural partitioning. The structure of interest is partitioned into two substructure-physical and numerical. The two

---

\*Corresponding author, Scientist, E-mail: [mohitverma@serc.res.in](mailto:mohitverma@serc.res.in)

<sup>a</sup>Chief Scientist

<sup>b</sup>Distinguished Emeritus Professor

substructures are made to interact with each other in such a way that they emulate the dynamic response of the structure of interest. The structural component whose behaviour is not well understood or cannot be modelled accurately is generally taken as the physical substructure. Since the test is carried out in real-time, RTHT helps to capture the rate dependent behaviour which is often difficult to model. The calculation of the displacement response, application of the displacement on the structural component, measurement and feedback of the reaction forces are done in a single time step. RTHT has been used to evaluate the dynamic response for various types of structural systems (tuned liquid damper (Lee *et al.* 2007), pantograph catenary (Facchinetti and Bruni 2012), coupled rotor blade - lag damper (Wallace *et al.* 2007)).

The integration schemes developed in the past for structural dynamics needs to be modified appropriately for RTHT. Blakeborough *et al.* (2001), have suggested that the computational overhead of the time integration scheme used in RTHT should be less for stability reasons. Therefore, explicit schemes should be preferred. Explicit schemes are conditionally stable and needs a short time step to ensure stability. Conditionally stable schemes are used only when the numerical substructure is limited to SDOF system (low natural frequency). Bonnet *et al.* (2008), have investigated and compared various time integration schemes used in RTHT. A multi-tasking strategy was also proposed within which the performance of various implicit and explicit algorithms was evaluated. Newmark explicit method was found to be computationally efficient and accurate within its stability region. Newmark-Chang method was found to be computationally more efficient than the operator splitting method (OSM) and was recommended for the cases where numerical stability could not be achieved with Newmark explicit scheme. The  $\alpha$ -OSM scheme was found to be efficient for numerical dissipation of the higher modes. The work carried out by Bonnet *et al.* (2008), did not concentrate on the stability limits and the accuracy of the results obtained through time integration methods for different damping ratios of the physical substructure which is being currently addressed in the present study. In the presence of a number of integration methods, it is preferable to have criteria for their selection. As such criteria are not available presently, this paper attempts to fill this gap by numerically assessing the four commonly used step-by-step methods, viz. Central difference method; Operator splitting method, Rosenbrock based method and CR-integration method in terms of stability and accuracy. In order to benchmark the performance of the step-by-step integration method, a non-dimensional error index has been defined. In order to carry out a comprehensive review five different cases, undamped SDOF, damped SDOF, instantaneous softening, instantaneous hardening and hysteretic system, have been studied. The first two examples assess the performance of the scheme in the linear while the other three in nonlinear regime. To cover a broad spectrum, three different types of nonlinearities are considered-softening, hardening and hysteresis in the present study. The present work will help in making a better decision for choosing a particular time integration method in the paradigm of RTHT.

## 2. Review of step-by-step integration methods

The dynamic behaviour of a SDOF system can be represented by the following equation

$$m\ddot{\mathbf{x}}(\mathbf{t}) + \mathbf{r}(\mathbf{x}, \dot{\mathbf{x}}) = \mathbf{f}(\mathbf{t}) \quad (1)$$

where  $m$  is the mass,  $\mathbf{r}$  is the restoring force,  $\mathbf{f}$  is the excitation force,  $\mathbf{x}$  is the displacement,  $\dot{\mathbf{x}}$  is the

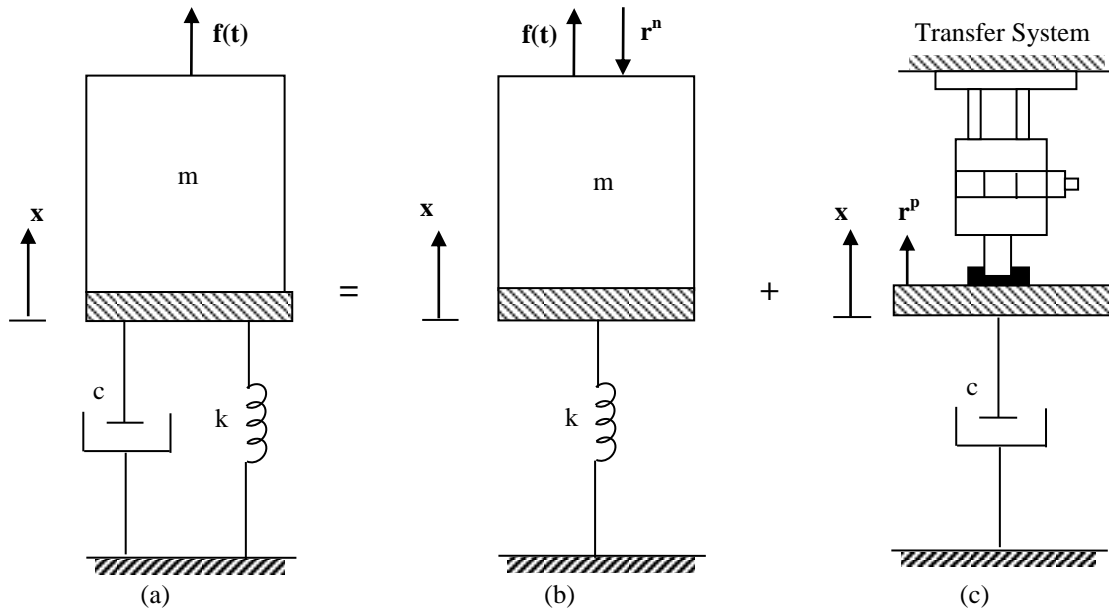


Fig. 1 Partitioning of a SDOF system-(a) Full system, (b) numerical substructure, (c) physical substructure

velocity and  $\ddot{\mathbf{x}}$  is the acceleration.

In the present study, SDOF system has been partitioned as shown in Fig. 1. Mass and stiffness are taken as the numerical substructure while damping alone is taken as the physical substructure.

Therefore, the Eq. (1) can be rewritten as

$$m\ddot{\mathbf{x}}(t) + \mathbf{r}^n + \mathbf{r}^p = \mathbf{f}(t) \tag{2}$$

$$\mathbf{r}^n = k\mathbf{x} \tag{3}$$

$$\mathbf{r}^p = c\dot{\mathbf{x}} \tag{4}$$

where the superscript **n** and **p** corresponds to the numerical and the physical substructure, respectively. The time discretized equation of the motion of substructured SDOF system at  $i^{\text{th}}$  time step can be written as

$$m\ddot{\mathbf{x}}_i + \mathbf{r}^n_i + \mathbf{r}^p_i = \mathbf{f}_i \tag{5}$$

The following section briefly describes some of the time integration schemes which have been selected for assessment.

### 2.1 Central difference method (CDM)

Central difference method (CDM) is an explicit method which is obtained by substituting the velocity and acceleration terms from the difference equations in the dynamic equations of motion

$$\mathbf{x}_{i+1} = \left(\frac{m}{\Delta t^2}\right)^{-1} \left[ \mathbf{f}_i - \left(k - \frac{2m}{\Delta t^2}\right)\mathbf{x}_i - \left(\frac{m}{\Delta t^2}\right)\mathbf{x}_{i-1} - c\dot{\mathbf{x}}_i \right] \tag{6}$$

$$\dot{\mathbf{x}}_{i+1} = \left(\frac{m}{\Delta t}\right)^{-1} \left[ \mathbf{f}_i - \left(k - \frac{m}{\Delta t^2}\right)\mathbf{x}_i - \left(\frac{m}{\Delta t^2}\right)\mathbf{x}_{i-1} - c\dot{\mathbf{x}}_i \right] \tag{7}$$

where  $\Delta t$  is the integration time step. This scheme has been widely used by many researchers (Nakashima *et al.* 1992, Shing *et al.* 1996, Horiuchi *et al.* 1999, Nakashima and Nobuaki 1999, Darby *et al.* 2001, Darby *et al.* 2002). Wu *et al.* (2005, 2009), have studied the stability and accuracy of central difference method (CDM) for RTHT.

## 2.2 Operator splitting method (OSM)

The mathematical formulation of the OSM is similar to the constant average acceleration method. OSM predicts the displacement and velocity by following equations

$$\tilde{x}_{i+1} = x_i + \Delta t \dot{x}_i + \frac{\Delta t^2}{4} \ddot{x}_i \quad (8)$$

$$\tilde{\dot{x}}_{i+1} = \dot{x}_i + \frac{\Delta t}{2} \ddot{x}_i \quad (9)$$

$$x_{i+1} = \tilde{x}_{i+1} + \frac{\Delta t^2}{4} \ddot{x}_{i+1} \quad (10)$$

$$\dot{x}_{i+1} = \tilde{\dot{x}}_{i+1} + \frac{\Delta t}{2} \ddot{x}_{i+1} \quad (11)$$

where  $\tilde{x}$  and  $\tilde{\dot{x}}$  are the predictor displacement and velocity, respectively.

Wu *et al.* (2006) have proposed an updated formulation of the OSM for application of the scheme to systems with non-linear damping.

## 2.3 Rosenbrock based method (RBM)

Bursi *et al.* (2008), have presented a real-time compatible time integration scheme based on Rosenbrock schemes. The work of Bursi *et al.* (2008), was further extended by Lamarche *et al.* (2009). Rosenbrock-W method was proposed in which the mechanical properties of the physical substructure were included in the Jacobian matrix. The stability and accuracy of the scheme were investigated in both linear as well as nonlinear regime. The scheme was found to be second order accurate in the nonlinear regime even when the initially assumed Jacobian matrix was not exact.

The state space equation of the system can be expressed as

$$\dot{\mathbf{y}} = \mathbf{f}(\mathbf{y}, \mathbf{t}) = \begin{bmatrix} \dot{\mathbf{x}} \\ \frac{1}{m}(-k\mathbf{x} - c\dot{\mathbf{x}}) \end{bmatrix} \quad (12)$$

where  $\mathbf{y} = [\mathbf{x} \ \dot{\mathbf{x}}]^T$  defines the state vectors. Rosenbrock method evaluates the states for the next time step based on the following equations

$$\mathbf{y}_{i+1} = \mathbf{y}_i + b_1 \mathbf{k}_1 + b_2 \mathbf{k}_2 \quad (13)$$

$$\mathbf{k}_1 = [\mathbf{I} - \gamma \Delta t \mathbf{J}]^{-1} \mathbf{f}(\mathbf{y}_i, \mathbf{t}_i) \Delta t \quad (14)$$

$$\mathbf{y}_{i+\alpha} = \mathbf{y}_i + \alpha \mathbf{k}_1 \quad (15)$$

$$\mathbf{k}_2 = [\mathbf{I} - \gamma \Delta t \mathbf{J}]^{-1} (\mathbf{f}(\mathbf{y}_{i+\alpha}, \mathbf{t}_{i+\alpha}) - \mathbf{J} \gamma \mathbf{k}_1) \Delta t \quad (16)$$

where  $b_1, b_2, \gamma, \alpha$  are algorithmic parameters and  $\mathbf{J}$  is the Jacobian matrix defined as

$$\mathbf{J} = \begin{bmatrix} 0 & 1 \\ -k/m & -c/m \end{bmatrix} \quad (17)$$

The following values are recommended for RTHT (Lamarche *et al.* 2009)

$$\alpha = 1/2, \quad b_1 = 0, \quad b_2 = 1, \quad \gamma = 1/2 \tag{18}$$

### 2.4 CR- integration

CR-integration method was proposed by Chen and Ricles (2008). The displacement and the velocity are predicted as

$$\mathbf{x}_{i+1} = \mathbf{x}_i + \Delta t \dot{\mathbf{x}}_i + \Delta t^2 d_2 \ddot{\mathbf{x}}_i \tag{19}$$

$$\dot{\mathbf{x}}_{i+1} = \dot{\mathbf{x}}_i + \Delta t d_1 \ddot{\mathbf{x}}_i \tag{20}$$

$$d = d_1 = d_2 = \frac{4m}{4m+2c\Delta t+k\Delta t^2} \tag{21}$$

where  $d_1$  and  $d_2$  are the integration parameters. The explicit nature and the second order accuracy of the CR-integration for displacement and velocity makes it ideal for RTHT. The accuracy and stability of the method was investigated by Chen and Ricles (2008), Chen *et al.* (2009), in both linear and nonlinear regime. It was demonstrated that the method is unconditionally stable as long as the system is of the softening type.

### 3. Stability analysis

Free vibration of the SDOF system is considered in order to analyse the stability of different time integration schemes. The stability of an algorithm can be evaluated from the free vibration solution. The states between the two adjacent time steps are related and written in the recursive form (Wu *et al.* 2005)

$$\mathbf{y}_{i+1} = \mathbf{A} \mathbf{y}_i \tag{22}$$

where  $y_i$  is the state of the system at  $i^{\text{th}}$  time step and  $A$  is the amplification matrix.

The stability of an algorithm depends upon the eigenvalues of the amplification matrix. A time integration scheme is said to be stable if the following condition is satisfied (Wu *et al.* 2005)

$$\rho(A) \leq 1 \tag{23}$$

where  $\rho(A)$  is the spectral radius of  $A$ . Spectral radius of a matrix is defined as the absolute maximum of the eigenvalues of the matrix. The amplification matrix for the different schemes is expressed in terms of  $\xi_E$ ,  $\Omega$  and  $\omega$  which are defined as (Wu *et al.* 2005)

$$\xi_E = \frac{c}{2m\omega} \tag{24}$$

$$\Omega = \omega\Delta t \tag{25}$$

$$\omega = \sqrt{\frac{k}{m}} \tag{26}$$

The next step involves the derivation of the amplification matrix for various schemes.

### 3.1 Amplification matrix for CDM

The state vector for CDM can be represented as (Wu *et al.* 2005)

$$\mathbf{y}_i = [\mathbf{x}_i, \mathbf{x}_{i-1}, \dot{\mathbf{x}}_i \Delta t]^T \quad (27)$$

Using Eq. (6), the displacement for the  $(i+1)^{\text{th}}$  step for a free vibration problem can be written as

$$\begin{aligned} \mathbf{x}_{i+1} &= \left(\frac{m}{\Delta t^2}\right)^{-1} \left[ -\left(k - \frac{2m}{\Delta t^2}\right) \mathbf{x}_i - \left(\frac{m}{\Delta t^2}\right) \mathbf{x}_{i-1} - c \dot{\mathbf{x}}_i \right] \\ &= -\left(\frac{k}{m} \Delta t^2 - 2\right) \mathbf{x}_i - \mathbf{x}_{i-1} - \frac{c}{m} \Delta t^2 \dot{\mathbf{x}}_i \\ &= (2 - \Omega^2) \mathbf{x}_i - \mathbf{x}_{i-1} - 2\xi_E \Omega \Delta t \dot{\mathbf{x}}_i \end{aligned} \quad (28)$$

$$\begin{aligned} \dot{\mathbf{x}}_{i+1} \Delta t &= \left(\frac{m}{\Delta t^2}\right)^{-1} \left[ -\left(k - \frac{m}{\Delta t^2}\right) \mathbf{x}_i - \left(\frac{m}{\Delta t^2}\right) \mathbf{x}_{i-1} - c \dot{\mathbf{x}}_i \right] \\ &= -\left(\frac{k}{m} \Delta t^2 - 1\right) \mathbf{x}_i - \mathbf{x}_{i-1} - \frac{c}{m} \Delta t^2 \dot{\mathbf{x}}_i \\ &= (1 - \Omega^2) \mathbf{x}_i - \mathbf{x}_{i-1} - 2\xi_E \Omega \Delta t \dot{\mathbf{x}}_i \end{aligned} \quad (29)$$

The equations can be represented in the matrix form as shown below

$$\begin{pmatrix} \mathbf{x}_{i+1} \\ \mathbf{x}_i \\ \dot{\mathbf{x}}_{i+1} \Delta t \end{pmatrix} = \begin{bmatrix} 2 - \Omega^2 & -1 & -2\xi_E \Omega \\ 0 & 1 & 0 \\ 1 - \Omega^2 & -1 & -2\xi_E \Omega \end{bmatrix} \begin{pmatrix} \mathbf{x}_i \\ \mathbf{x}_{i-1} \\ \dot{\mathbf{x}}_i \Delta t \end{pmatrix} \quad (30)$$

$$\mathbf{A} = \begin{bmatrix} 2 - \Omega^2 & -1 & -2\xi_E \Omega \\ 0 & 1 & 0 \\ 1 - \Omega^2 & -1 & -2\xi_E \Omega \end{bmatrix} \quad (31)$$

Similar expression is obtained if we substitute the damping ratio of the numerical substructure as zero in the expression obtained by Wu *et al.* (2005).

### 3.2 Amplification matrix for OSM

The state vectors for OSM are given below (Wu *et al.* 2006)

$$\mathbf{y}_i = [\tilde{\mathbf{x}}_i, \tilde{\mathbf{x}}_i \Delta t, \ddot{\mathbf{x}}_i \Delta t^2]^T \quad (32)$$

Using Eqs. (10) and (11), the displacement and velocity for the  $i^{\text{th}}$  step can be written as

$$\mathbf{x}_i = \tilde{\mathbf{x}}_i + \frac{\Delta t^2}{4} \ddot{\mathbf{x}}_i \quad (33)$$

$$\dot{\mathbf{x}}_i = \tilde{\mathbf{x}}_i + \frac{\Delta t}{2} \ddot{\mathbf{x}}_i \quad (34)$$

Substituting the expression for  $x_i$  and  $\dot{x}_i$  in Eq. (8)

$$\tilde{\mathbf{x}}_{i+1} = \tilde{\mathbf{x}}_i + \frac{\Delta t^2}{4} \ddot{\mathbf{x}}_i + \Delta t \left( \tilde{\mathbf{x}}_i + \frac{\Delta t}{2} \ddot{\mathbf{x}}_i \right) + \frac{\Delta t^2}{4} \ddot{\mathbf{x}}_i = \tilde{\mathbf{x}}_i + \tilde{\mathbf{x}}_i \Delta t + \ddot{\mathbf{x}}_i \Delta t^2 \quad (35)$$

Multiplying Eq. (9) with  $\Delta t$  and substituting expression for  $\dot{\mathbf{x}}_i$

$$\tilde{\mathbf{x}}_{i+1}\Delta t = \left(\tilde{\mathbf{x}}_i + \frac{\Delta t}{2}\dot{\mathbf{x}}_i\right)\Delta t + \frac{\Delta t^2}{2}\ddot{\mathbf{x}}_i = \tilde{\mathbf{x}}_i\Delta t + \dot{\mathbf{x}}_i\Delta t^2 \quad (36)$$

The discretized equation of motion at  $(i+1)^{\text{th}}$  step can be written as

$$m\ddot{\mathbf{x}}_{i+1} + c\dot{\mathbf{x}}_{i+1} + k\mathbf{x}_{i+1} = 0 \quad (37)$$

Eq. (27) can be represented in the following form using Eq. (26)

$$\ddot{\mathbf{x}}_{i+1} + 2\xi_E\omega\dot{\mathbf{x}}_{i+1} + \omega^2\mathbf{x}_{i+1} = 0 \quad (38)$$

Using Eqs. (35) and (36) and simplifying we get the following equations

$$\ddot{\mathbf{x}}_{i+1} + 2\xi_E\omega\left(\tilde{\mathbf{x}}_{i+1} + \frac{\Delta t}{2}\dot{\mathbf{x}}_{i+1}\right) + \omega^2\left(\tilde{\mathbf{x}}_{i+1} + \frac{\Delta t^2}{4}\ddot{\mathbf{x}}_{i+1}\right) = 0 \quad (39)$$

$$\ddot{\mathbf{x}}_{i+1} + 2\xi_E\omega\left(\tilde{\mathbf{x}}_i + \dot{\mathbf{x}}_i\Delta t + \frac{\Delta t}{2}\ddot{\mathbf{x}}_{i+1}\right) + \omega^2\left(\tilde{\mathbf{x}}_i + \tilde{\mathbf{x}}_i\Delta t + \dot{\mathbf{x}}_i\Delta t^2 + \frac{\Delta t^2}{4}\ddot{\mathbf{x}}_{i+1}\right) = 0 \quad (40)$$

$$\ddot{\mathbf{x}}_{i+1}\left(1 + \xi_E\omega\Delta t + \frac{\omega^2\Delta t^2}{4}\right) + \omega^2\tilde{\mathbf{x}}_i + (2\xi_E\omega + \omega^2\Delta t)\tilde{\mathbf{x}}_i + (2\xi_E\omega\Delta t + \omega^2\Delta t^2)\dot{\mathbf{x}}_i = 0 \quad (41)$$

$$\ddot{\mathbf{x}}_{i+1}\Delta t^2 = -\left(\frac{\Omega^2\tilde{\mathbf{x}}_i + (2\xi_E\Omega + \Omega^2)\tilde{\mathbf{x}}_i\Delta t + (2\xi_E\Omega + \Omega^2)\dot{\mathbf{x}}_i\Delta t^2}{1 + \xi_E\Omega + \frac{\Omega^2}{4}}\right) \quad (42)$$

In matrix form, the equations can be represented as

$$\begin{pmatrix} \tilde{\mathbf{x}}_{i+1} \\ \tilde{\mathbf{x}}_{i+1}\Delta t \\ \ddot{\mathbf{x}}_{i+1}\Delta t^2 \end{pmatrix} = \begin{bmatrix} 1 & 1 & 1 \\ 0 & 1 & 1 \\ -\frac{\Omega^2}{1 + \xi_E\Omega + \Omega^2/4} & -\frac{2\Omega\xi_E + \Omega^2}{1 + \xi_E\Omega + \Omega^2/4} & -\frac{2\Omega\xi_E + \Omega^2}{1 + \xi_E\Omega + \Omega^2/4} \end{bmatrix} \begin{pmatrix} \tilde{\mathbf{x}}_i \\ \tilde{\mathbf{x}}_i\Delta t \\ \ddot{\mathbf{x}}_i\Delta t^2 \end{pmatrix} \quad (43)$$

$$\mathbf{A} = \begin{bmatrix} 1 & 1 & 1 \\ 0 & 1 & 1 \\ -\frac{\Omega^2}{1 + \xi_E\Omega + \Omega^2/4} & -\frac{2\Omega\xi_E + \Omega^2}{1 + \xi_E\Omega + \Omega^2/4} & -\frac{2\Omega\xi_E + \Omega^2}{1 + \xi_E\Omega + \Omega^2/4} \end{bmatrix} \quad (44)$$

Similar expression is obtained if we substitute the damping ratio of the numerical substructure as zero in the expression obtained by Wu *et al.* (2005).

### 3.3 Amplification matrix for RBM

The state vector of the Rosenbrock scheme is given below

$$\mathbf{y}_i = [\mathbf{x} \ \dot{\mathbf{x}}]^T \quad (45)$$

The amplification matrix for the Rosenbrock scheme was derived by Lemarche *et al.* (2009), by neglecting damping. The amplification matrix arrived at in the present study takes into account the damping of the physical substructure.

Eq. (12) can also be represented as

$$\dot{\mathbf{y}} = \mathbf{f}(\mathbf{y}_i, \mathbf{t}_i) = \mathbf{J}\mathbf{y}_i \quad (46)$$

Using Eqs. (14) and (46),

$$\mathbf{k}_1 = [\mathbf{I} - \gamma\Delta t\mathbf{J}]^{-1}\mathbf{J}\mathbf{y}_i\Delta t \quad (47)$$

Substituting  $\alpha = \frac{1}{2}$  in Eq. (15)

$$\mathbf{y}_{i+\frac{1}{2}} = \mathbf{y}_i + \frac{1}{2}\mathbf{k}_1 \quad (48)$$

Using Eqs. (16), (47) and (48)

$$\begin{aligned} \mathbf{k}_2 &= [\mathbf{I} - \gamma\Delta t\mathbf{J}]^{-1} \left( \mathbf{f} \left( \mathbf{y}_{i+\frac{1}{2}}, \mathbf{t}_{i+\frac{1}{2}} \right) - \mathbf{J}\gamma\mathbf{k}_1 \right) \Delta t \\ &= [\mathbf{I} - \gamma\Delta t\mathbf{J}]^{-1} \left( \mathbf{J}\mathbf{y}_i + \frac{1}{2}\mathbf{J}\mathbf{k}_2 - \mathbf{J}\gamma\mathbf{k}_1 \right) \Delta t \\ &= [\mathbf{I} - \gamma\Delta t\mathbf{J}]^{-1} \left( 1 + \left( \frac{1}{2} - \gamma \right) [\mathbf{I} - \gamma\Delta t\mathbf{J}]^{-1}\mathbf{J}\Delta t \right) \mathbf{J}\mathbf{y}_i\Delta t \end{aligned} \quad (49)$$

From Eqs. (13), (18) and (49) we get the following equations

$$\mathbf{y}_{i+1} = \mathbf{y}_i + \mathbf{k}_2 \quad (50)$$

$$\mathbf{y}_{i+1} = \mathbf{y}_i \left\{ [\mathbf{I} - \gamma\Delta t\mathbf{J}]^{-1} \left( 1 + \left( \frac{1}{2} - \gamma \right) [\mathbf{I} - \gamma\Delta t\mathbf{J}]^{-1}\mathbf{J}\Delta t \right) \mathbf{J}\Delta t \right\} \quad (51)$$

$$\mathbf{A} = \left\{ [\mathbf{I} - \gamma\Delta t\mathbf{J}]^{-1} \left( 1 + \left( \frac{1}{2} - \gamma \right) [\mathbf{I} - \gamma\Delta t\mathbf{J}]^{-1}\mathbf{J}\Delta t \right) \mathbf{J}\Delta t \right\} \quad (52)$$

After simplification, the amplification matrix is obtained as

$$\mathbf{A} = \frac{1}{2(1+2\xi_E\gamma\Omega+\gamma^2\Omega^2)^2} \begin{bmatrix} A_{11} & A_{12} \\ A_{21} & A_{22} \end{bmatrix} \quad (53)$$

where,  $A_{11} = 2(1 + 2\xi_E\gamma\Omega + \gamma^2\Omega^2)^2 - \Omega^2 - 4\gamma^3\Omega^4 + \Omega^3\gamma^2(\Omega - 4\xi_E)$

$A_{12} = [(6\gamma^2 - 2\gamma)\Omega^2 + 2\xi_E(4\gamma - 1)\Omega + 2]\Delta t$

$A_{21} = \omega\Omega((2\gamma - 6\gamma^2)\Omega^2 - 2\xi_E(4\gamma - 1)\Omega - 2)$

$$\begin{aligned} A_{22} &= 4\Omega^2\xi_E^2 - 4\Omega\xi_E - \gamma^2(16\xi_E\Omega^3 - \Omega^4) + 2(\gamma^2\Omega^2 + 2\xi_E\gamma\Omega + 1)^2 - \Omega^2 \\ &\quad - 2\gamma(8\Omega^2\xi_E^2 - 2\Omega^3\xi_E) - 4\gamma^3\Omega^4 \end{aligned}$$

### 3.4 Amplification matrix for CR-integration

The state vector of the CR-integration scheme (Chen *et al.* 2008), is represented as

$$\mathbf{y}_i = [\mathbf{x}_i, \dot{\mathbf{x}}_i\Delta t]^T \quad (54)$$

The discretized equation of motion at the  $i^{\text{th}}$  step can be written as

$$m\ddot{\mathbf{x}}_i + c\dot{\mathbf{x}}_i + k\mathbf{x}_i = 0 \quad (55)$$

$$\ddot{\mathbf{x}}_i + 2\xi_E\omega\dot{\mathbf{x}}_i + \omega^2\mathbf{x}_i = 0 \quad (56)$$

$$\ddot{\mathbf{x}}_i = -2\xi_E\omega\dot{\mathbf{x}}_i - \omega^2\mathbf{x}_i \quad (57)$$

From Eqs. (19) and (57),

$$\begin{aligned} \mathbf{x}_{i+1} &= \mathbf{x}_i + \Delta t \dot{\mathbf{x}}_i + \Delta t^2 d(-2\xi_E \omega \dot{\mathbf{x}}_i - \omega^2 \mathbf{x}_i) \\ &= (1 - \omega^2 \Delta t^2 d) \mathbf{x}_i + (1 - 2d\xi_E \omega \Delta t) \dot{\mathbf{x}}_i \Delta t \\ &= (1 - \Omega^2 d) \mathbf{x}_i + (1 - 2d\xi_E \Omega) \dot{\mathbf{x}}_i \Delta t \end{aligned} \tag{58}$$

Similarly, from Eqs. (20) and (57)

$$\begin{aligned} \dot{\mathbf{x}}_{i+1} \Delta t &= \dot{\mathbf{x}}_i \Delta t + \Delta t^2 d(-2\xi_E \omega \dot{\mathbf{x}}_i - \omega^2 \mathbf{x}_i) \\ &= (-\omega^2 \Delta t^2 d) \mathbf{x}_i + (1 - 2d\xi_E \omega \Delta t) \dot{\mathbf{x}}_i \Delta t \\ &= (-\Omega^2 d) \mathbf{x}_i + (1 - 2d\xi_E \Omega) \dot{\mathbf{x}}_i \Delta t \end{aligned} \tag{59}$$

Expressing Eqs. (58) and (59) in matrix form

$$\begin{pmatrix} \mathbf{x}_{i+1} \\ \dot{\mathbf{x}}_{i+1} \Delta t \end{pmatrix} = \begin{bmatrix} 1 - d\Omega^2 & 1 - 2d\xi_E \Omega \\ -d\Omega^2 & 1 - 2d\xi_E \Omega \end{bmatrix} \begin{pmatrix} \mathbf{x}_i \\ \dot{\mathbf{x}}_i \Delta t \end{pmatrix} \tag{60}$$

$$\mathbf{A} = \begin{bmatrix} 1 - d\Omega^2 & 1 - 2d\xi_E \Omega \\ -d\Omega^2 & 1 - 2d\xi_E \Omega \end{bmatrix} \tag{61}$$

Table 1 Amplification matrix for different integration methods

Method	State vector	Amplification matrix
CDM	$[\mathbf{x}_i, \mathbf{x}_{i-1}, \dot{\mathbf{x}}_i \Delta t]^T$	$\begin{bmatrix} 2 - \Omega^2 & -1 & -2\xi_E \Omega \\ 0 & 1 & 0 \\ 1 - \Omega^2 & -1 & -2\xi_E \Omega \end{bmatrix}$ $\begin{bmatrix} 1 & 1 & 1 \\ 0 & 1 & 1 \\ -a2 & -a1 & -a1 \end{bmatrix}$
OSM	$[\tilde{\mathbf{x}}_i, \tilde{\mathbf{x}}_i \Delta t, \tilde{\mathbf{x}}_i \Delta t]^T$	$a1 = \frac{2\Omega\xi_E + \Omega^2}{1 + \xi_E \Omega + \Omega^2/4}$ $a2 = \frac{\Omega^2}{1 + \xi_E \Omega + \Omega^2/4}$ $\frac{1}{2(1 + 2\xi_E \gamma \Omega + \gamma^2 \Omega^2)^2} \begin{bmatrix} A_{11} & A_{12} \\ A_{21} & A_{22} \end{bmatrix}$
RBM	$[\mathbf{x} \ \dot{\mathbf{x}}]^T$	$A_{11} = 2(1 + 2\xi_E \gamma \Omega + \gamma^2 \Omega^2)^2 - \Omega^2 - 4\gamma^3 \Omega^4 + \Omega^3 \gamma^2 (\Omega - 4\xi_E)$ $A_{12} = [(6\gamma^2 - 2\gamma)\Omega^2 + 2\xi_E(4\gamma - 1)\Omega + 2]\Delta t$ $A_{21} = \omega\Omega((2\gamma - 6\gamma^2)\Omega^2 - 2\xi_E(4\gamma - 1)\Omega - 2)$ $A_{22} = 4\Omega^2 \xi_E^2 - 4\Omega \xi_E - \gamma^2(16\xi_E \Omega^3 - \Omega^4) + 2(\gamma^2 \Omega^2 + 2\xi_E \gamma \Omega + 1)^2 - \Omega^2 - 2\gamma(8\Omega^2 \xi_E^2 - 2\Omega^3 \xi_E) - 4\gamma^3 \Omega^4$
CR	$[\mathbf{x}_i, \dot{\mathbf{x}}_i \Delta t]^T$	$\begin{bmatrix} 1 - d\Omega^2 & 1 - 2d\xi_E \Omega \\ -d\Omega^2 & 1 - 2d\xi_E \Omega \end{bmatrix}$ $d = \frac{4}{4 + 4\Omega\xi_E + \Omega^2}$

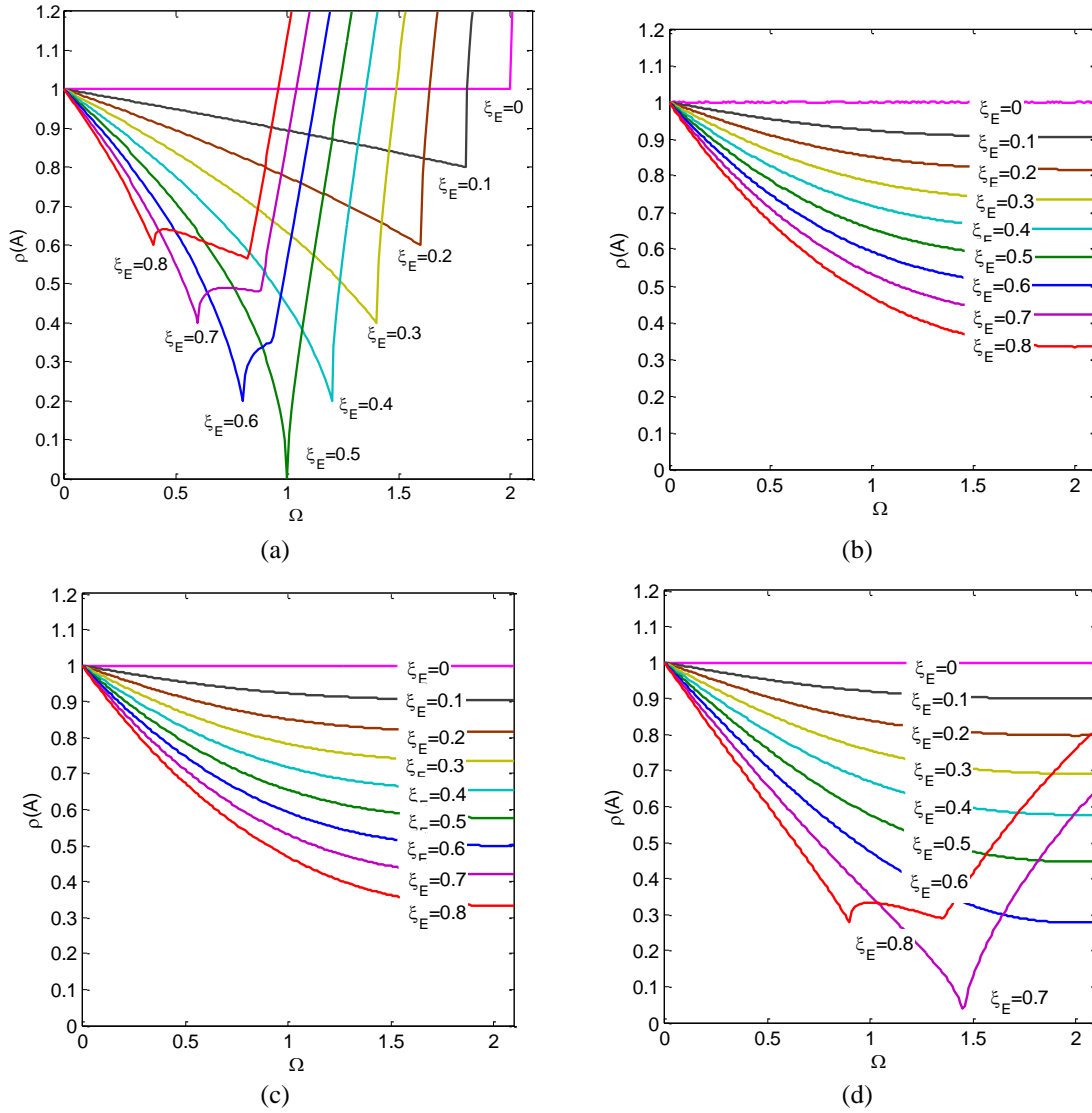


Fig. 2 Spectral radii - (a) CDM, (b) OSM, (c) RBM, (d) CR

The state vector and the amplification matrix for the different time integration methods are summarized in Table 1. The spectral radius of the amplification matrix for different methods is plotted for various values of  $\Omega$  and  $\xi_E$ . The plots obtained are shown in Fig. 2. The plots obtained for CDM and OSM are found to be in agreement with those reported in the literature.

Based on Fig. 2, it can be inferred that:

(a) The stability limit  $\Omega$  for CDM decreases with the increase in the damping ratio of the physical substructure which is given by (Wu *et al.* 2005)

$$\Omega < \sqrt{4 + 4\xi_E^2} - 2\xi_E \tag{62}$$

(b) The spectral radii of OSM, Rosenbrock and CR integration methods is less than unity for all the cases. Thus, it is demonstrated that these schemes are unconditionally stable for RTHT.

#### 4. Accuracy analysis

The accuracy of an integration algorithm is quantified in terms of period distortion and numerical damping which are derived from the eigenvalues of the amplification matrix.

The complex eigenvalue ( $\lambda$ ) of the amplification matrix can be expressed as (Wu *et al.* 2005)

$$\lambda = a \pm ib \tag{63}$$

$$\lambda = \exp((- \hat{\xi} \pm i)\bar{\Omega}) \tag{64}$$

where,

$$\hat{\xi} = -\frac{\ln(a^2+b^2)}{2\bar{\Omega}} \tag{65}$$

$$\bar{\Omega} = \arctan\left(\frac{b}{a}\right) \tag{66}$$

The displacement response for a free vibration case can be expressed as (Wu *et al.* 2005)

$$\mathbf{x}_n = \exp(-\hat{\xi}\bar{\omega}\mathbf{n}\Delta t)(c_1 \cos\bar{\omega}\mathbf{n}\Delta t + c_2 \sin\bar{\omega}\mathbf{n}\Delta t) \tag{67}$$

where,  $\bar{\omega} = \bar{\Omega}/\Delta t$ . The values of the constants  $c_j$  are determined from the initial conditions. For a free vibration case, the closed form solution for displacement response of viscously underdamped system can be written as (Wu *et al.* 2005)

$$\mathbf{x}_n = \exp(-\hat{\xi}\bar{\omega}_n\mathbf{n}\Delta t)(c_1 \cos\bar{\omega}_d\mathbf{n}\Delta t + c_2 \sin\bar{\omega}_d\mathbf{n}\Delta t) \tag{68}$$

where

$$\xi = \frac{\hat{\xi}}{\sqrt{1+\hat{\xi}^2}} \tag{69}$$

$$\bar{\omega}_d = \bar{\omega} \tag{70}$$

$$\bar{\omega}_n = \frac{\bar{\omega}_d}{\sqrt{1-\xi^2}} \tag{71}$$

The numerical damping ratio is defined as

$$\bar{\xi} = \xi - \xi_E \tag{72}$$

The period distortion for the damped system is expressed as

$$\frac{\Delta T_d}{T_d} = \frac{T_d - \bar{T}_d}{T_d} = 1 - \frac{\omega_d}{\bar{\omega}_d} = 1 - \frac{\Omega}{\bar{\Omega}} \sqrt{1 - \xi_E^2} \tag{73}$$

The numerical damping ratio and period distortion of various methods are plotted for different values of damping ratio of the physical substructure. The plots are shown in Figs. 3 and 4.

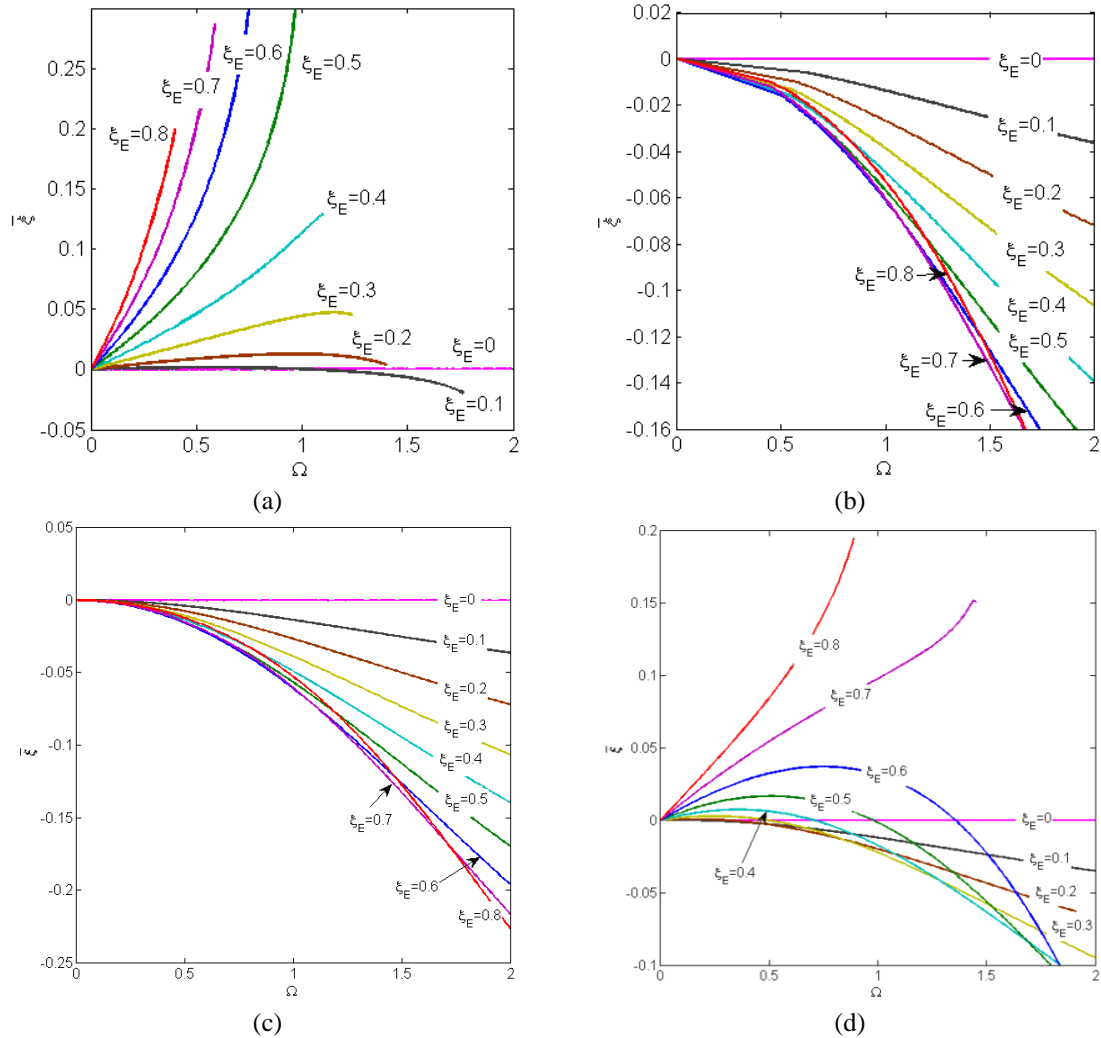


Fig. 3 Numerical damping - (a) CDM, (b) OSM, (c) RBM, (d) CR

Based on Figs. 3 and 4, following observations have been made:

(a) The numerical damping ratio of CDM increases with the increase in the damping ratio of the physical substructure. The period distortion is also found to increase up to a value of 0.5 damping ratio after which it starts decreasing.

(b) The behavior of OSM and RBM is found to be similar in nature. Numerical damping is negative for all the damping ratios considered in the present study. The absolute value of the numerical damping increases with the increase in the damping of the physical substructure. Period distortion is also found to increase with the increase in the damping ratio of the physical substructure.

(c) The numerical damping of CR integration decreases up to 0.3 damping ratio after which it starts increasing. In general, period distortion is found to increase with the increase in the damping ratio of the physical substructure.

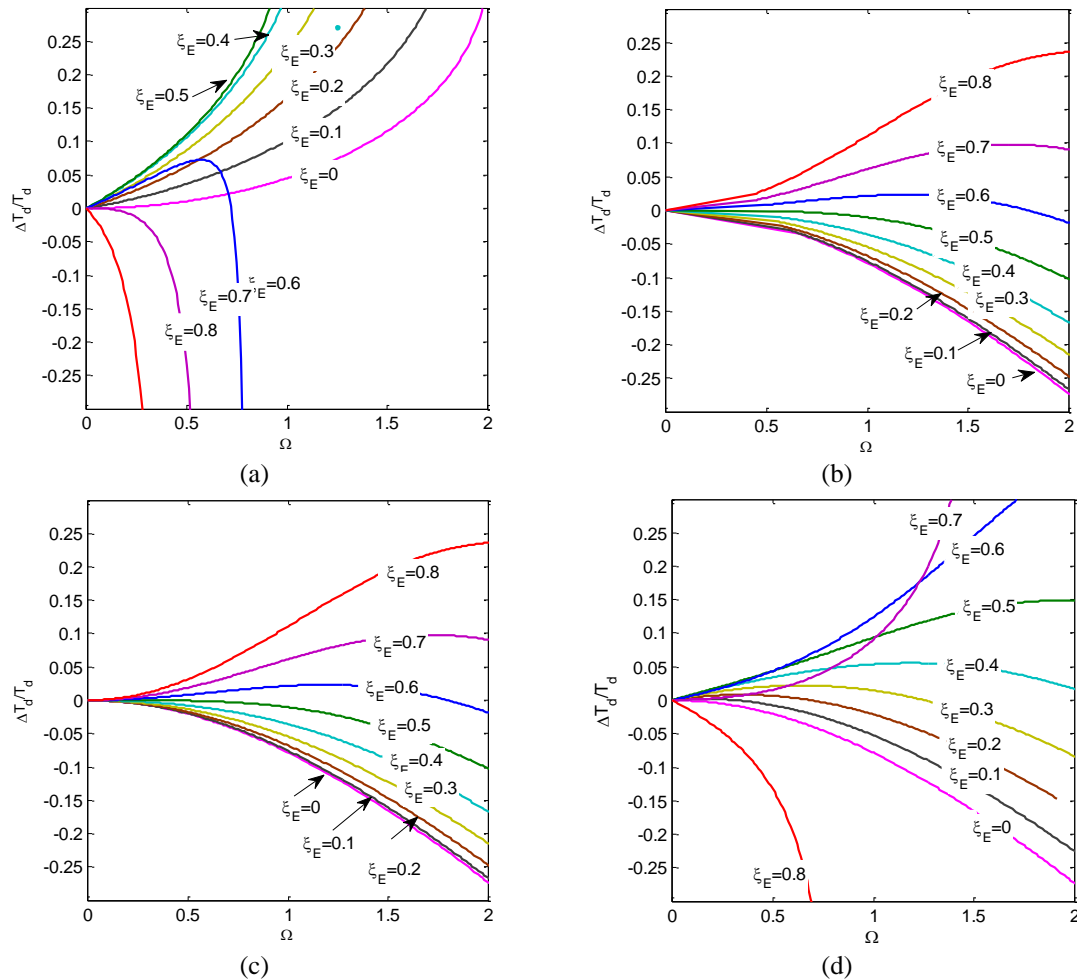


Fig. 4 Period distortion - (a) CDM, (b) OSM, (c) RBM, (d) CR

### 5. Numerical assessment

In order to assess the different methods of time integration for RTHT, different examples are studied. The examples have been chosen so as to cover the wide range of structure which can be encountered in case of RTHT. The first two examples considers linear physical substructure while the last three considers nonlinear physical substructure. In the nonlinear regime, three different types of nonlinearities are considered for comprehensive assessment.

#### 5.1 Example 1: Undamped SDOF system

The system considered has 100 kg mass and 16100 N/m stiffness. Since there is no damping, stiffness alone is taken as physical substructure. The system is subjected to unit displacement and zero initial velocity. The equation of motion of the system and initial conditions can be represented using the following second order differential equation

$$\frac{d^2x}{dt^2} + \frac{16100}{100}x = 0, x(0) = 1, \dot{x}(0) = 0 \tag{74}$$

The closed form solution of the system is evaluated by solving the above differential equation. The solution obtained is referred to as the exact solution and is given by the following equation

$$x = \cos(\sqrt{161}t) \tag{75}$$

The simulation of the system response using different time integration methods has been carried out using different time steps as listed in Table 2. The displacement response and displacement-velocity phase plots obtained using different time integration methods is compared with the exact solution in Figs. 5 and 6, respectively.

In order to quantify the performance of the method, the following error index ( $e$ ) is defined

$$e = \frac{\|y_i - y\|}{\|y\|} \cdot 100 \tag{76}$$

where  $y_i$  and  $y$  are the response vector obtained from the time integration method and exact solution, respectively. The displacement and velocity error index obtained for different time steps are given in Table 2.

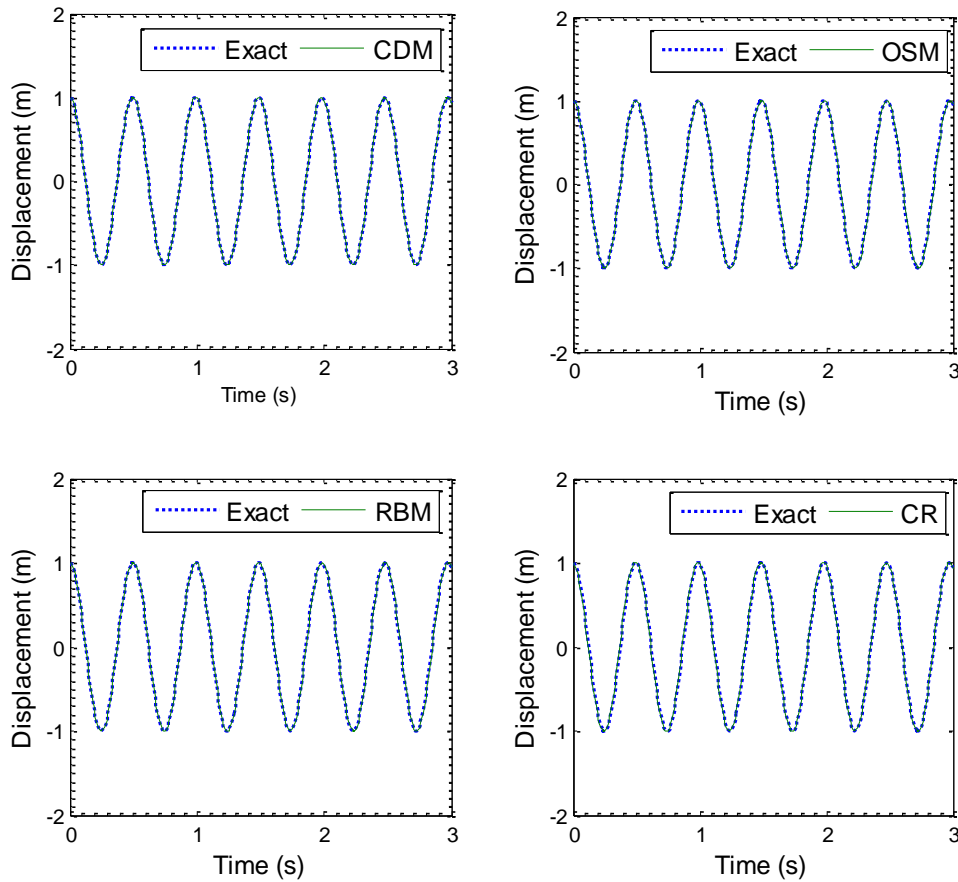


Fig. 5 Comparison of displacement response for undamped SDOF system ( $\Delta t = 0.01$  s)

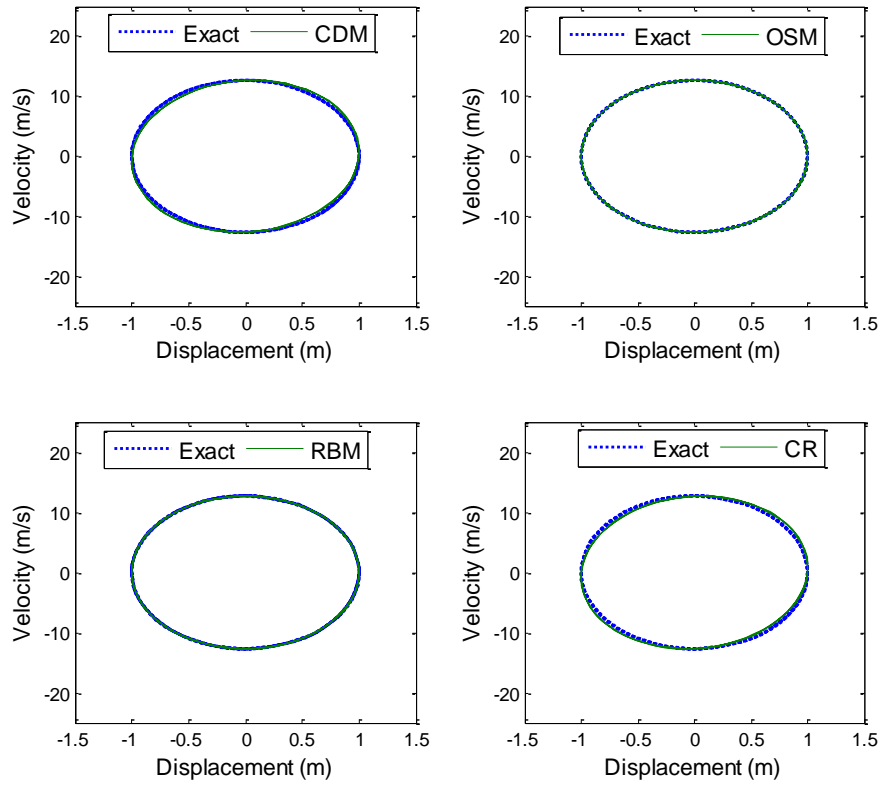


Fig. 6 Displacement-velocity phase plot for undamped SDOF system ( $\Delta t = 0.01s$ )

Table 2 Error indices for undamped SDOF system

$\Delta t$ (s)	Displacement error index				Velocity error index			
	CDM	OSM	RBM	CR	CDM	OSM	RBM	CR
0.010	1.4466	2.8837	2.8837	4.0402	5.1501	3.0040	3.0040	3.0040
0.009	1.1721	2.3381	2.3381	3.8087	4.7410	2.4281	2.4281	2.4281
0.008	0.9257	1.8476	1.8476	3.5422	4.3125	1.9233	1.9233	1.9233
0.007	0.7091	1.4161	1.4161	3.2493	3.8567	1.4679	1.4679	1.4679
0.006	0.5207	1.0403	1.0403	2.9127	3.3819	1.0819	1.0819	1.0819
0.005	0.3617	0.7227	0.7227	2.5398	2.8806	0.7513	0.7513	0.7513
0.004	0.2315	0.4627	0.4627	2.1245	2.3548	0.4808	0.4808	0.4808
0.003	0.1302	0.2604	0.2604	1.6646	1.8042	0.2704	0.2704	0.2704
0.002	0.0579	0.1158	0.1158	1.1582	1.2284	0.1201	0.1201	0.1201
0.001	0.0145	0.0289	0.0289	0.6038	0.6271	0.0300	0.0300	0.0300

### 5.2 Example 2: Damped SDOF system

The system considered is similar to the one used in example 1 except viscous damping of 127 Ns/m is introduced. The equation of motion of the system and initial conations are given by

$$\frac{d^2x}{dt^2} + \frac{127}{100} \frac{dx}{dt} + \frac{16100}{100} x = 0, x(0) = 1, \dot{x}(0) = 0 \tag{77}$$

The solution of the above differential equation is found to be

$$x = e^{\frac{-127t}{200}} \left[ \cos\left(\frac{\sqrt{6423871}t}{200}\right) + \frac{127}{\sqrt{6423871}} \sin\left(\frac{\sqrt{6423871}t}{200}\right) \right] \tag{78}$$

The displacement and velocity error index is calculated in the same way as it was calculated for example 1 and is summarized in Table 3. The comparison of the displacement response with the exact solution for different methods is shown in Fig. 7. The comparison of the displacement-velocity phase plot is shown in Fig. 8.

Table 3 Error indices for damped SDOF system

$\Delta t$ (s)	Displacement error index				Velocity error index			
	CDM	OSM	RBM	CR	CDM	OSM	RBM	CR
0.010	4.6380	1.6174	1.6174	5.1850	4.2246	1.6518	1.6518	1.6518
0.009	4.1026	1.3108	1.3108	4.7555	3.8024	1.3371	1.3371	1.3371
0.008	3.5837	1.0365	1.0365	4.3084	3.3831	1.0571	1.0571	1.0571
0.007	3.0800	0.7940	0.7940	3.8439	2.9626	0.8086	0.8086	0.8086
0.006	2.5927	0.5838	0.5838	3.3595	2.5439	0.5946	0.5946	0.5946
0.005	2.1211	0.4056	0.4056	2.8553	2.1239	0.4129	0.4129	0.4129
0.004	1.6652	0.2598	0.2598	2.3300	1.7030	0.2642	0.2642	0.2642
0.003	1.2252	0.1462	0.1462	1.7826	1.2806	0.1486	0.1486	0.1486
0.002	0.8010	0.0650	0.0650	1.2123	0.8563	0.0660	0.0660	0.0660
0.001	0.3926	0.0163	0.0163	0.6184	0.4296	0.0165	0.0165	0.0165

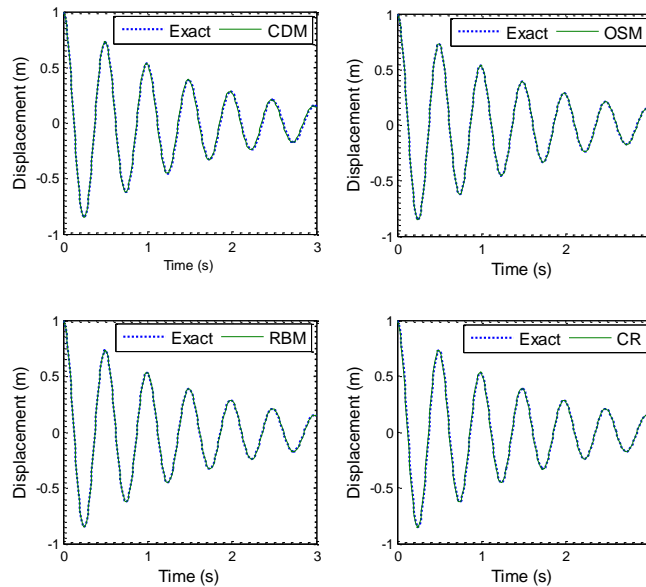


Fig. 7 Comparison of displacement response for damped SDOF system ( $\Delta t=0.01s$ )

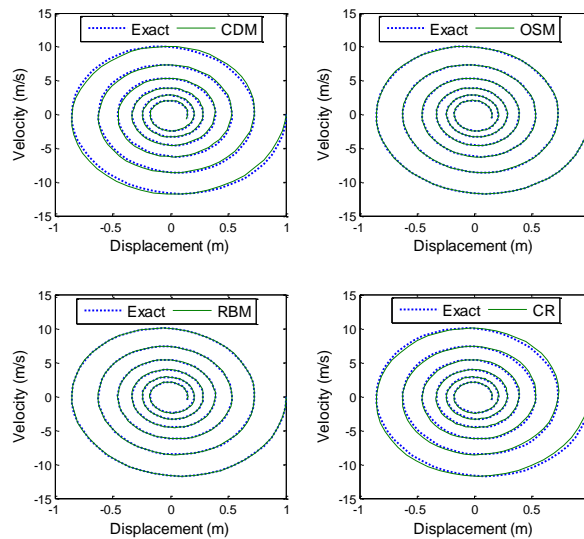


Fig. 8 Displacement-velocity phase plot for damped SDOF system ( $\Delta t=0.01s$ )

### 5.3 Example 3: Instantaneous softening

The system consists of a two storey shear building (Fig. 9). The stiffness of the upper storey is subjected to instantaneous softening which is modelled using the following equation

$$k_2 = k_0 \left( 1 + \alpha \sqrt{|\Delta u|} \right) \tag{79}$$

Where  $k_0$  is the initial stiffness and  $|\Delta u|$  is the inter storey drift. Since the behaviour of upper storey is nonlinear, it is taken as physical substructure while the bottom storey is assumed to behave linearly and is taken as numerical substructure. The example has been adopted from Chang (2009). The properties of the system are given in Table 4. The dynamic response of the system is evaluated for the base acceleration of  $50 \sin(5t)$  where  $t$  is the time in seconds. The displacement time histories and the phase plots obtained for the upper storey using different time integration schemes for 0.01s time step are shown in Fig. 10. The corresponding displacement-velocity phase plots are shown in Fig. 11. The error index is calculated based on the Eq. (76) and is given in Table 5 for different time steps of integration. The exact solution of the system is obtained using ode15s in Matlab.

Table 4 Properties for the shear building model

Parameter	Value
$m_1$ (kg)	$10^4$
$m_2$ (kg)	$10^3$
$k_1$ (N/m)	$10^8$
$k_0$ (N/m)	$10^5$
$\alpha$ (Example 3)	-0.2
$\alpha$ (Example 4)	0.2

Table 5 Error indices for instantaneous softening

$\Delta t$ (s)	Displacement error index				Velocity error index			
	CDM	OSM	RBM	CR	CDM	OSM	RBM	CR
0.010	7.5669	4.8668	3.2295	1.2862	8.0516	6.9959	4.2874	5.0832
0.009	6.8121	4.4047	2.9402	1.0394	7.2383	6.3120	3.9009	4.4308
0.008	6.0552	3.9457	2.6476	0.8224	6.4615	5.6658	3.5253	3.8117
0.007	5.2945	3.4670	2.3496	0.6281	5.6473	4.9706	3.1308	3.2249
0.006	4.5378	2.9924	2.0442	0.4619	4.8490	4.2879	2.7286	2.6723
0.005	3.7812	2.5101	1.7308	0.3204	4.0507	3.5983	2.3161	2.1506
0.004	3.0248	2.0236	1.4072	0.2049	3.2467	2.8989	1.8861	1.6607
0.003	2.2681	1.5273	1.0737	0.1148	2.4355	2.1839	1.4403	1.2013
0.002	1.5116	1.0255	0.7283	0.0512	1.6278	1.4670	0.9793	0.7725
0.001	0.7559	0.5168	0.3710	0.0127	0.8157	0.7388	0.4997	0.3722

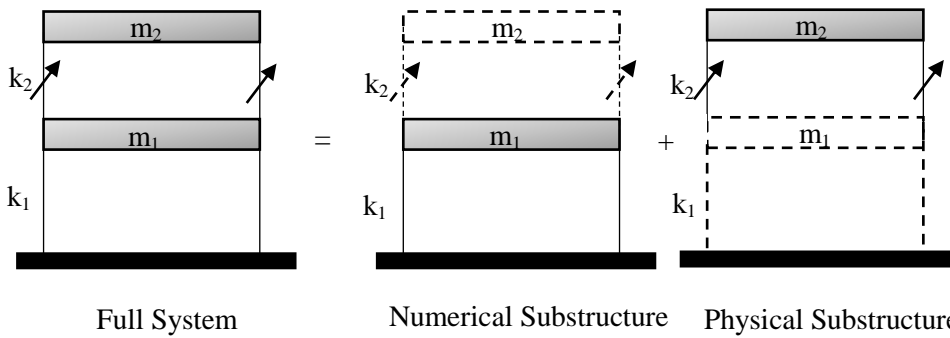


Fig. 9 Model of the structure considered for instantaneous softening and hardening case

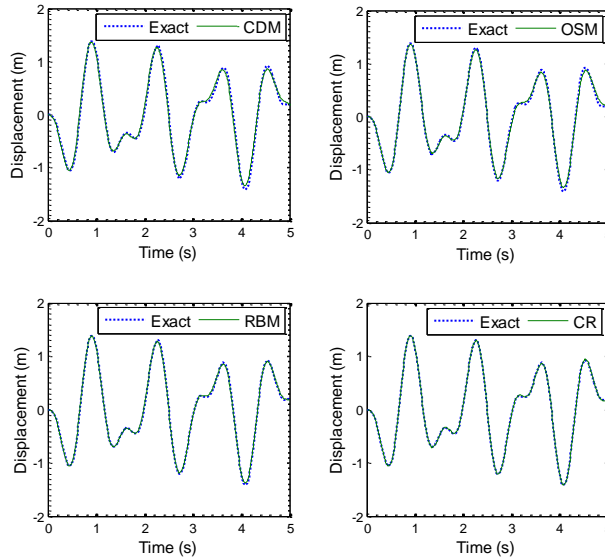


Fig. 10 Comparison of displacement response for instantaneous softening ( $\Delta t=0.01s$ )

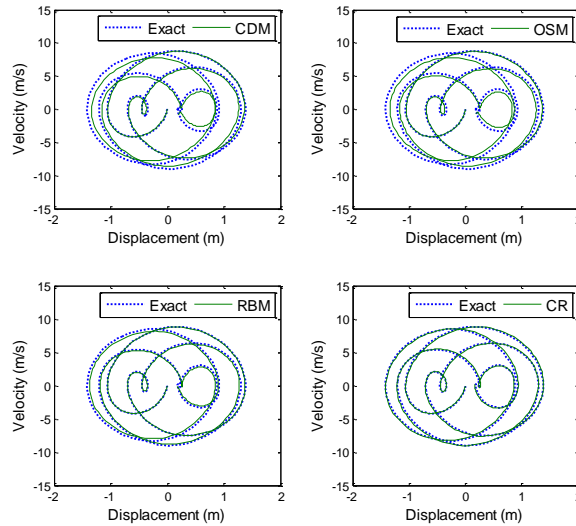


Fig. 11 Displacement-velocity phase plot for instantaneous softening ( $\Delta t=0.01s$ )

#### 5.4 Example 4: Instantaneous hardening

The system considered is same as the previous example. The hardening behaviour is modelled by modifying the parameter  $\alpha$  in example 3. A positive value of  $\alpha$  is chosen to simulate instantaneous hardening system. The dynamic response of the system is evaluated for the two different time steps. The displacement time histories and the phase plots obtained for the upper storey using different time integration schemes are shown in Figs. 18 to 21. The error indices calculated for different time steps are given in Table 7. The exact solution of the system in this case also is obtained using ode15s in Matlab.

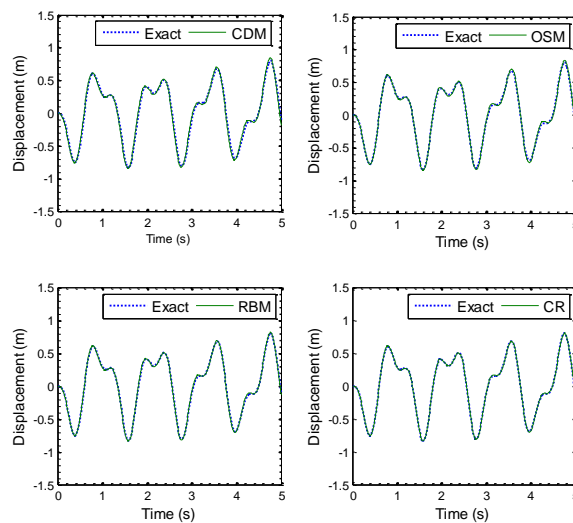


Fig. 12 Comparison of displacement response for instantaneous hardening ( $\Delta t = 0.01s$ )

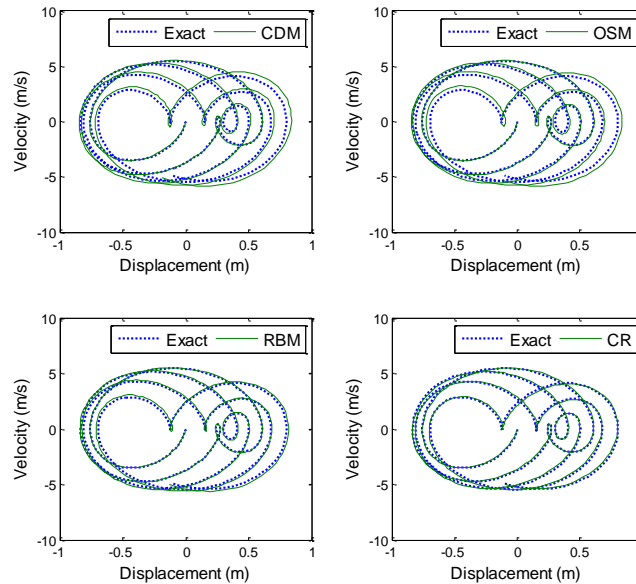
Fig. 13 Displacement-velocity phase plot for instantaneous hardening ( $\Delta t=0.01s$ )

Table 6 Error indices for instantaneous hardening

$\Delta t$ (s)	Displacement error index				Velocity error index			
	CDM	OSM	RBM	CR	CDM	OSM	RBM	CR
0.010	8.1233	3.7797	3.3460	0.9941	8.1671	6.4942	4.4502	5.5198
0.009	7.2427	3.3494	3.0339	0.8038	7.2962	5.7550	4.0586	4.8459
0.008	6.4068	2.9329	2.7311	0.6358	6.4049	5.0437	3.6543	4.1922
0.007	5.5623	2.5362	2.4142	0.4865	5.5577	4.3619	3.2458	3.5730
0.006	4.7320	2.1452	2.0944	0.3573	4.7116	3.6896	2.8273	2.9804
0.005	3.9202	1.7679	1.7691	0.2482	3.8863	3.0397	2.3949	2.4148
0.004	3.1143	1.4026	1.4344	0.1587	3.0790	2.4106	1.9505	1.8780
0.003	2.3178	1.0432	1.0888	0.0890	2.2887	1.7925	1.4892	1.3692
0.002	1.5362	0.6910	0.7366	0.0397	1.5101	1.1860	1.0105	0.8865
0.001	0.7630	0.3437	0.3736	0.0098	0.7479	0.5895	0.5151	0.4302

### 5.5 Example 5: Hysteretic system

The system considered in this case is a three storey frame equipped with the lead rubber dampers in the bracing of the 1<sup>st</sup> storey (Fig. 14). The frame is taken as the numerical substructure while the lead rubber bearing is taken as physical substructure. The properties of the structure has been adopted from Lu and Zhou (2002). It is assumed that the lead rubber bearing is installed only in the 1<sup>st</sup> storey. The hysteretic behaviour of the lead rubber bearings is simulated by using Bouc-Wen model (Wen 1976). The restoring force obtained by solving the Bouc-Wen model equations was given to the different time integration schemes as the restoring force corresponding to the physical substructure. The properties of the structure and the parameters of the Bouc-Wen model

are also adopted from Lu and Qiang (2002). The frame is subjected to the North-South component of the El-Centro 1940 earthquake record with 0.35 g peak ground acceleration (PGA), and the displacement of the 1<sup>st</sup> storey is evaluated based on different time integration schemes. The time step of the integration was taken as 0.01s. The exact solution is obtained using ode15s in Matlab. The displacement time history and phase plot for the 1<sup>st</sup> storey are shown in Figs. 15 and 16. The hysteresis curve for the lead rubber bearing is shown in Fig. 17. The error indices for the different time integration schemes are given in Table 7.

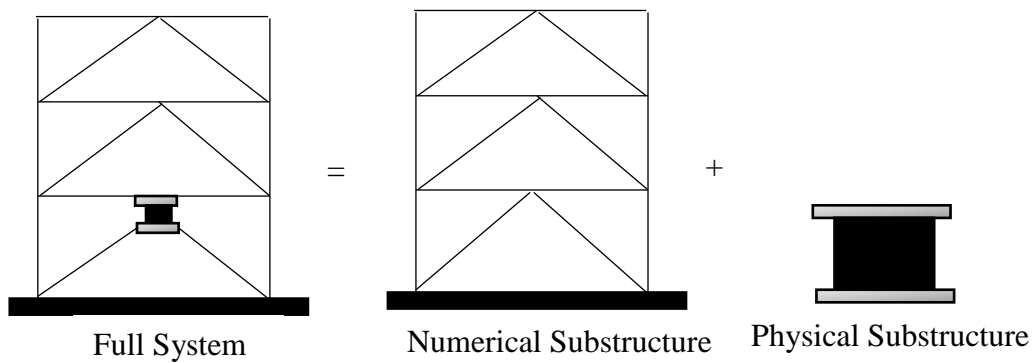


Fig. 14 Model of the structure considered for hysteretic system case

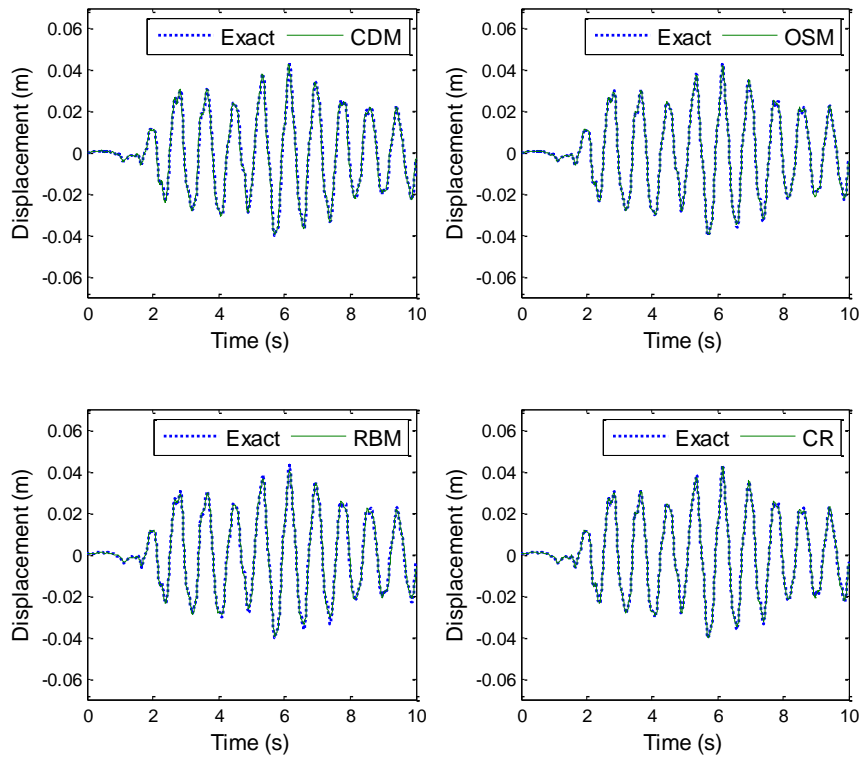


Fig. 15 Comparison of displacement response for hysteretic system ( $\Delta t=0.01s$ )

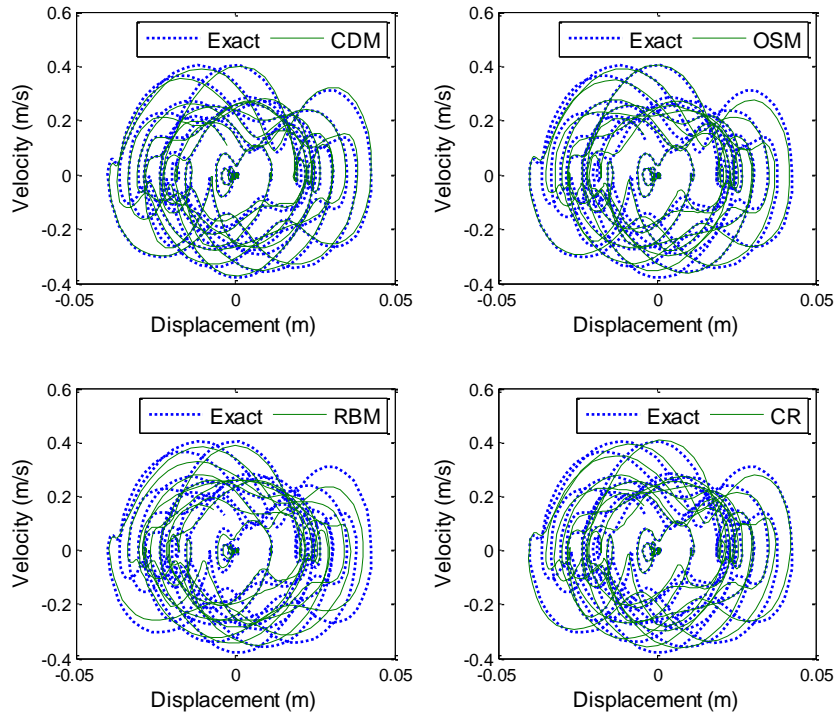


Fig. 16 Displacement-velocity phase plot for hysteretic system ( $\Delta t = 0.01s$ )

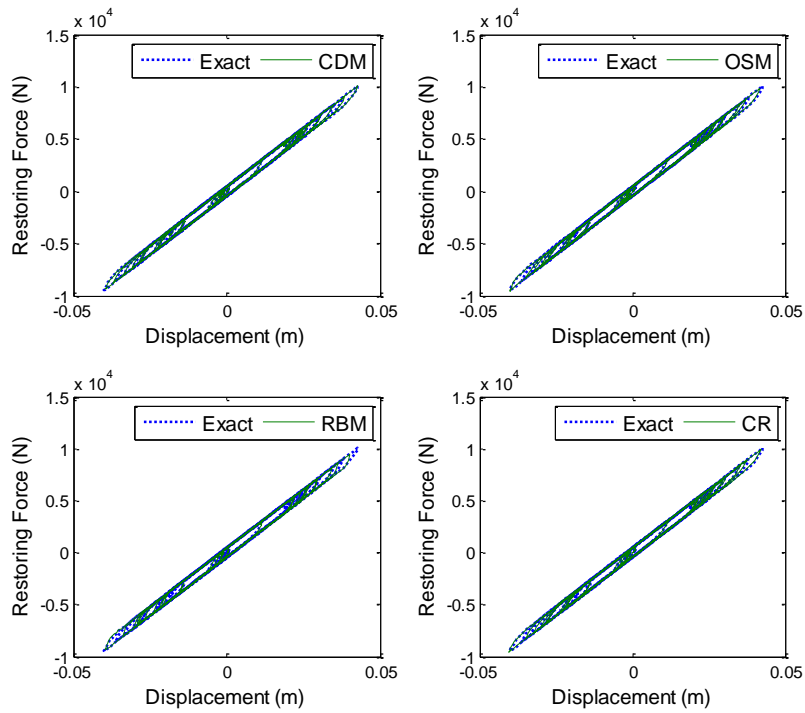


Fig. 17 Displacement-velocity phase plot for hysteretic system ( $\Delta t = 0.01s$ )

Table 7 Error indices for hysteretic system

$\Delta t$ (s)	Displacement error index				Velocity error index			
	CDM	OSM	RBM	CR	CDM	OSM	RBM	CR
0.010	10.0202	3.4724	6.8105	3.4498	15.5545	12.2715	21.4739	17.9087

Table 8 Summary of the stability and accuracy analysis

	Accuracy order	Unconditional Stability	Numerical damping	Period distortion
<b>CDM</b>	2 <sup>nd</sup>	No	Yes	Yes
<b>OSM</b>	2 <sup>nd</sup>	Yes	Yes	Yes
<b>RBM</b>	2 <sup>nd</sup>	Yes	Yes	Yes
<b>CR</b>	2 <sup>nd</sup>	Yes	Yes	Yes

## 6. Conclusions

The assessment of the four different time integration schemes that are widely used for real-time hybrid testing (RTHT) has been carried out. The schemes have been assessed on the basis of stability and accuracy for different damping ratios of the physical substructure. The summary of the stability and accuracy analysis for a linear system is given in Table 8.

Based on the stability analysis, it has been observed that CDM is conditionally stable where as OSM, RBM and CR are unconditionally stable. The accuracy analysis suggested that the trend in numerical damping and period distortion is similar for OSM and RBM. In order to evaluate the performance of the different step-by-step integration methods, five example studies have been carried out. The examples have been selected so as to cover the wide range of physical substructures that one may encounter in RTHT. The first two examples studied the performance of the integration method in linear regime. The first two example considered a SDOF system with and without damping. The third and fourth examples have been selected to study the performance of the integration method in the nonlinear regime. Example three and four studied the effect of the instantaneous softening and hardening on the accuracy of the time integration method. The fifth example consisted of a nonlinear hysteretic system. The hysteretic behaviour has been represented using Bouc-Wen model. The error indices obtained for the different examples gives as indication of the accuracy of the integration method. The indices help in making an informed choice of the time integration method for a particular type of physical substructure. CDM is found to perform well only for undamped SDOF system. OSM and RBM are found to be robust and performed fairly well in all the examples studied. Though CR integration performed well for the nonlinear systems, it is unconditionally stable as long as the system is of the softening type. Therefore, its usage should be limited to only system showing softening behaviour.

## References

- Blakeborough, A., Williams, M.S., Darby, A.P. and Williams, D.M. (2001), "The development of real-time substructure testing", *Philosoph. Trans. Roy. Soc. London, Series A: Math. Phys. Eng. Sci.*, **359**(1786), 1869-1891.

- Bonnet, P.A., Williams, M.S. and Blakeborough, A. (2008), "Evaluation of numerical time-integration schemes for real-time hybrid testing", *Earthq. Eng. Struct. Dyn.*, **37**(13), 1467-1490.
- Bursi, O.S., Gonzalez-Buelga, A., Vulcan, L., Neild, S.A. and Wagg, D.J. (2008), "Novel coupling Rosenbrock-based algorithms for real-time dynamic substructure testing", *Earthq. Eng. Struct. Dyn.*, **37**(3), 339-360.
- Chang, S.Y. (2009), "Nonlinear evaluations of unconditionally stable explicit algorithms", *Earthq. Eng. Eng. Vib.*, **8**(3), 329-340.
- Chen, C. and Ricles, J.M. (2008), "Development of direct integration algorithms for structural dynamics using discrete control theory", *J. Eng. Mech.*, **134**(8), 676-683.
- Chen, C., Ricles, J.M., Marullo, T.M. and Mercan, O. (2009), "Real-time hybrid testing using the unconditionally stable explicit CR integration algorithm", *Earthq. Eng. Struct. Dyn.*, **38**(1), 23-44.
- Cheng, Chen and Ricles, J.M. (2008), "Development of direct integration algorithms for structural dynamics using discrete control theory", *J. Eng. Mech.*, **134**(8), 676-683.
- Darby, A.P., Blakeborough, A. and Williams, M.S. (2001), "Improved control algorithm for real-time substructure testing", *Earthq. Eng. Struct. Dyn.*, **30**(3), 431-448.
- Darby, A.P., Williams, M.S. and Blakeborough, A. (2002), "Stability and delay compensation for real-time substructure testing", *J. Eng. Mech.*, **128**(12), 1276-1284.
- Facchinetti, A. and Bruni, S. (2012), "Hardware-in-the-loop hybrid simulation of pantograph-catenary interaction", *J. Sound Vib.*, **331**(12), 2783-2797.
- Horiuchi, T., Inoue, M., Konno, T. and Namita, Y. (1999), "Real-time hybrid experimental system with actuator delay compensation and its application to a piping system with energy absorber", *Earthq. Eng. Struct. Dyn.*, **28**(10), 1121-1141.
- Lamarche, C.P., Bonelli, A., Bursi, O.S. and Tremblay, R. (2009), "A Rosenbrock-W method for real-time dynamic substructuring and pseudo-dynamic testing", *Earthq. Eng. Struct. Dyn.*, **38**(9), 1071-1092.
- Lee, S.K., Park, E.C., Min, K.W., Lee, S.H., Chung, L. and Park, J.H. (2007), "Real-time hybrid shaking table testing method for the performance evaluation of a tuned liquid damper controlling seismic response of building structures", *J. Sound Vib.*, **302**(3), 596-612.
- Lu, X. and Zhou, Q. (2002), "Dynamic analysis method of a combined energy dissipation system and its experimental verification", *Earthq. Eng. Struct. Dyn.*, **31**(6), 1251-1265.
- Nakashima, M. and Masaoka, N. (1999), "Real-time on-line test for MDOF systems", *Earthq. Eng. Struct. Dyn.*, **28**(4), 393-420.
- Nakashima, M., Kato, H. and Takaoka, E. (1992), "Development of real-time pseudo dynamic testing", *Earthq. Eng. Struct. Dyn.*, **21**(1), 79-92.
- Shing, P.B., Nakashima, M. and Bursi, O.S. (1996), "Application of pseudodynamic test method to structural research", *Earthq. Spectra*, **12**(1), 29-56.
- Wallace, M.I., Wagg, D.J., Neild, S.A., Bunniss, P., Lieven, N.A.J. and Crewe, A.J. (2007), "Testing coupled rotor blade-lag damper vibration using real-time dynamic substructuring", *J. Sound Vib.*, **307**(3), 737-754.
- Wen, Y.K. (1976), "Method for random vibration of hysteretic systems", *J. Eng. Mech. Div.*, **102**(2), 249-263.
- Wu, B., Bao, H., Ou, J. and Tian, S. (2005), "Stability and accuracy analysis of the central difference method for real-time substructure testing", *Earthq. Eng. Struct. Dyn.*, **34**(7), 705-718.
- Wu, B., Deng, L. and Yang, X. (2009), "Stability of central difference method for dynamic real-time substructure testing", *Earthq. Eng. Struct. Dyn.*, **38**(14), 1649-1663.
- Wu, B., Xu, G., Wang, Q. and Williams, M.S. (2006), "Operator-splitting method for real-time substructure testing", *Earthq. Eng. Struct. Dyn.*, **35**(3), 293-314.